ACS APPLIED MATERIALS & INTERFACES

Research Article

www.acsami.org

Peanut-Shell-like Porous Carbon from Nitrogen-Containing Poly-*N*-phenylethanolamine for High-Performance Supercapacitor

Xianjun Wei,* Suige Wan, Xiaoqiang Jiang, Zhe Wang, and Shuyan Gao*

Collaborative Innovation Center of Henan Province for Green Manufacturing of Fine Chemicals, Key Laboratory of Green Chemical Media and Reactions (Ministry of Education), School of Chemistry and Chemical Engineering, Henan Normal University, Xinxiang Henan 453007, People's Republic of China

Supporting Information

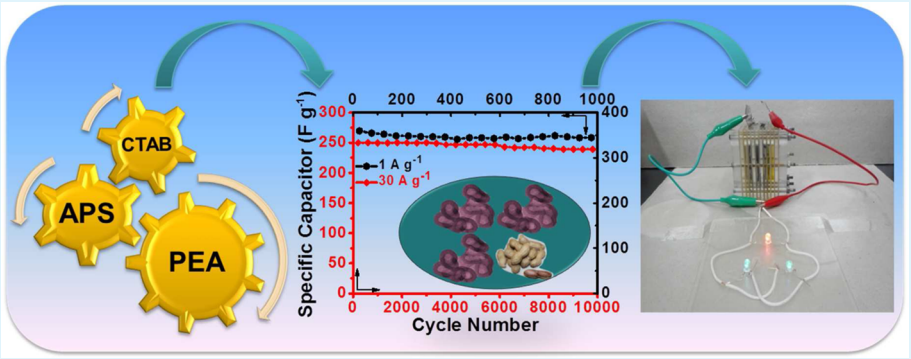

ABSTRACT: An efficient soft-template method is proposed for the synthesis of peanut shell-like porous carbon as high-performance supercapacitor electrode materials. The procedure is based on the pyrolysis and chemical activation processes using *N*-phenylethanolamine as precursor and KOH as activation agent. In a three-electrode system, the resultant carbon material has a specific capacitance of 356 F g^{-1} at 1 A g^{-1} and a good stability over 1000 cycles. Besides, at a high current density of 30 A g^{-1}, it has a specific capacitance of 249 F g^{-1} and maintains 96% after 10 000 cycles. In two-electrode cell configuration, it delivers about 21.53 Wh kg^{-1} at a current density of 20 A g^{-1}, which is about 7 times higher than the commercial device (<3 Wh kg^{-1}). Both high specific capacitance and excellent cycling stabilities guarantee its utilization in supercapacitors.

KEYWORDS: *conducting polymer, nitrogen-doping, supercapacitor, energy density, power density*

INTRODUCTION

Over the past 20 years, there has been a dramatic increase in research on porous materials. Their pore size and structure are required to be controllable to meet the demands of different applications. Although the original study mainly centers on silica or other oxides based on template techniques,[1] porous carbon materials seem to be more popular owing to the following two reasons: (1) the precursors for preparation of porous carbon materials are diverse and cost-effective and (2) carbon materials are naturally good biocompatibility, chemical stability, high conductivity, and mechanical strength. In view of these advantages, porous carbon materials find various applications in catalyst carriers,[2] carbon dioxide storages,[3] fuel cells,[4] and supercapacitors,[5,6] among which, the research on supercapacitors is getting more and more popular due to energy and environmental crises.[7] The pore size of activated carbons can be controlled by using different carbon precursors,[8,9] activated temperatures,[10] and activated methods.[11,12] More recently, Lv et al. treated ordered mesoporous carbon FDU-15 by KOH activation via adjusting the mass ratio and activation time, which resulted in a high specific surface area (SSA) and pore volume of 1410 m^2 g^{-1} and 0.73 cm^3 g^{-1}, respectively. The sample shows a good capacitor performance of 200 F g^{-1} at a current density of 0.5 A g^{-1}.[13] Although some physical and chemical activation procedures are applied to increase SSA to improve the electrochemical properties,[14] how to effectually regulate and control the pore structures still remains vital for the specific capacitance.

Additionally, it has been well documented that the capacitance of the carbon materials can be greatly improved by doping with heteroatoms (such as N, P, and B et al.) owing to the pseudocapacitive contribution.[15] Researchers have long been trying to search for new materials. For example, Ferrero et al. have adopted KOH-activation to obtain N-doped hollow carbon spheres, and the SSA increases to 2470 m^2 g^{-1} from 1500 m^2 g^{-1}, yet the specific capacitance (240 F g^{-1} at a low discharge rate of 0.1 A g^{-1}) seems not encouraging as expected.[16] Although many other related studies have observed exciting results, the preparation technology is fussy and needs drastic post-treatment.[17,18]

Received: June 8, 2015
Accepted: September 23, 2015
Published: September 23, 2015

DOI: 10.1021/acsami.5b05022
ACS Appl. Mater. Interfaces 2015, 7, 22238−22245

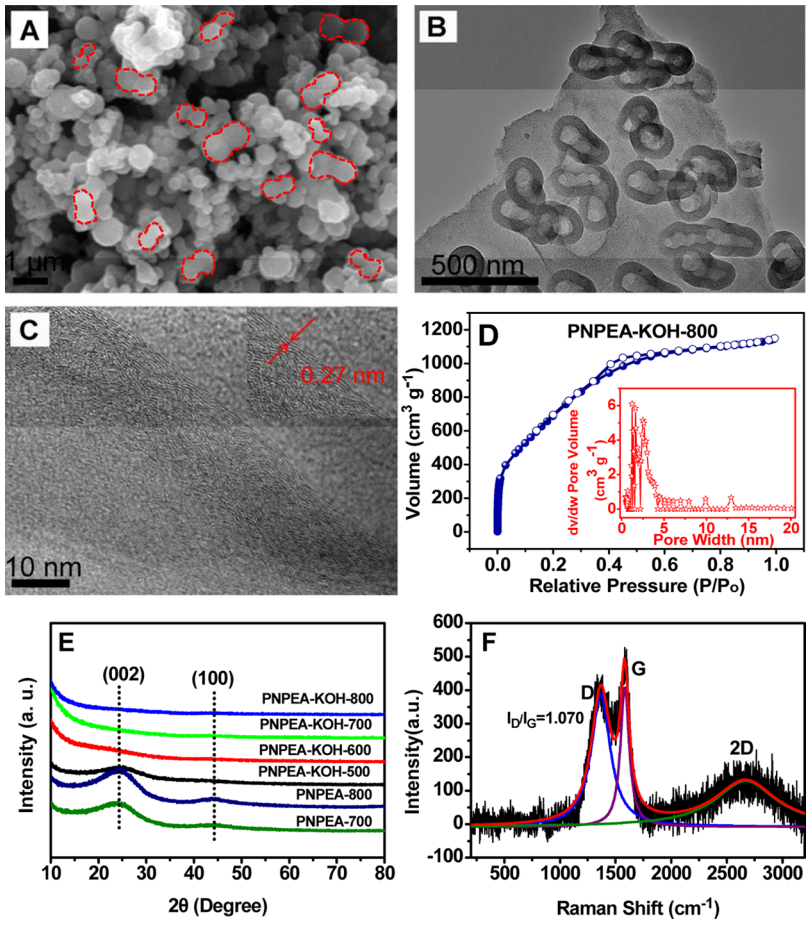

Figure 1. (A) SEM, (B) TEM, and (C) HRTEM images of PNPEA-KOH-800; (D) Ar adsorption−desorption isotherm of PNPEA-KOH-800 and pore-size distribution of NLDFT method (the inset); (E) XRD patterns of PNPEA-T and PNPEA-KOH-T carbons; and (F) Raman spectra of PNPEA-KOH-800.

Herein, we present an efficient soft-template method for the fabrication of N-doped microporous carbon materials. First, we employ *N*-phenylethanolamine (PEA) as the N-rich precursor to synthesize a conducting polymer, poly-*N*-phenylethanolamine (PNPEA) through one-pot method. Next, carbonization and activation of PNPEA resulted in a series of porous N-doped carbon materials. The as-prepared materials are denoted as PNPEA-KOH-T, where T stands for the carbonization temperature. In the three-electrode system, the obtained sample PNPEA-KOH-800 exhibits a high specific capacitance of 356 F g^{-1} at a current density of 1 A g^{-1} in 1 mol L^{-1} H_2SO_4, which is superior to many KOH-activated carbons.[19] In the two-electrode cell system, PNPEA-KOH-800 exhibits 248 F g^{-1} at 1 A g^{-1}, which also surpasses that of the commercially available activated carbon (240 F g^{-1}) and can be comparable to other carbon materials.[20,17]

EXPERIMENTAL SECTION

Materials. PEA (98%) was Alfa Aesar reagent and vacuum distilled before use, ammonium peroxydisulfate (APS, 98%) was purchased from Deen Tianjin Chemical Reagent Co., Ltd., hexadecyltrimethylammonium bromide (CTAB, 99%) and potassium hydroxide (KOH, 85%) were bought from Sinopharm Chemical Reagent Co., Ltd., Shanghai.

Preparation of PNPEA. First, 2.5 mmol of PEA and CTAB were dissolved in 40 mL of distilled water under magnetic stirring, into which 0.05 mol L^{-1} HCl (5 mL) was added. Two hours later, 0.5 mol L^{-1} APS (2.5 mmol) aqueous solution was added dropwise into the mixture. After standing at room temperature for 12 h, the product (PNPEA) was separated by filtration, washed with ethanol and water, and dried in an oven at 45 °C overnight under vacuum.

Preparation of Porous Carbon Samples. In our work, KOH was employed as the activation agent.[21] For all runs, 2 g KOH was added to 5 mL of deionized water containing 0.5 g PNPEA powder, then the resulting mixture was dried at 105 °C for 24 h after ceaselessly stirring 12 h at room temperature. Keeping stirring could promote the K^+ and OH^- penetrating into PNPEA powder, which lays the groundwork for following activation process. Since PNPEA is a lightweight powder, it is difficult for PNPEA powder and a high concentration solution of potassium hydroxide to wet each other in short time. Keeping long time stirring, such as 12 h, is a very important process. Selecting the stirring time is based on relevant reports[22,23] and our experiences. Afterward, the dried mass was placed in a nickel boat for carbonization in a tube furnace under N_2 gas flow. Typically, The furnace was heated from ambient temperature to the target temperature (500, 600, 700, and 800 °C) at 5 °C/min, maintained for 2 h under nitrogen gas flow, and finally cooled to room temperature automatically. The resulting dark solid was steeped with 2 mol L^{-1} HCl solution, followed by washing with copious amounts of deionized water until the pH was about neutral and dried in an oven at 80 °C for 24 h. The carbonized materials are denoted as PNPEA-KOH-T, where T stands for the carbonization temperature.

Structural Characterization. The structures of PNPEA-KOH-T were visualized by scanning electron microscopy (SEM, JSM-6390LV) and transmission electron microscopy (TEM, a JEOL JEM-2100 microscope). Argon or nitrogen adsorption and desorption curves were performed at 87.29 or 77.36 K by a Micromeritics ASAP 2020 volumetric instrument. The related parameters such as SSA, pore

DOI: 10.1021/acsami.5b05022
ACS Appl. Mater. Interfaces 2015, 7, 22238−22245

Scheme 1. Probable Formation Mechanism of the Peanut-Shell-like Porous Carbon

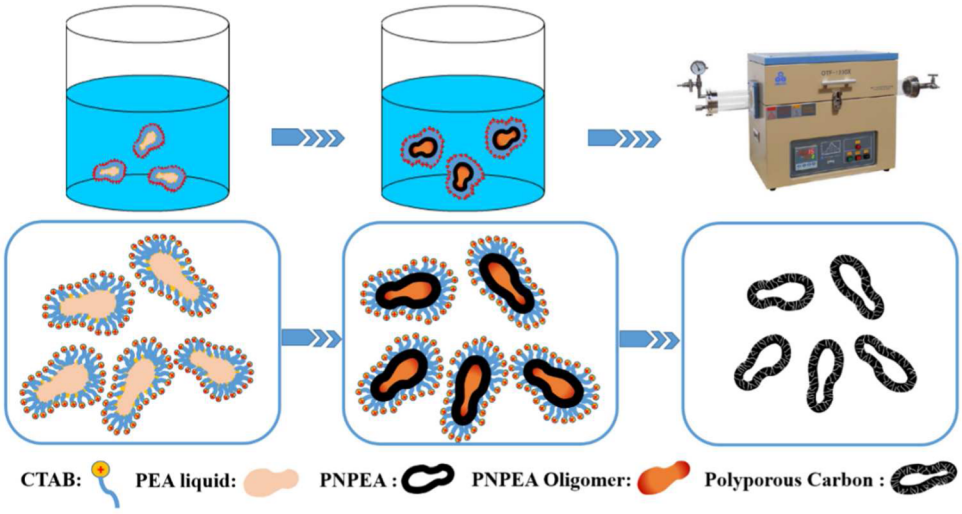

volume and pore size distribution can be acquired. The powder X-ray diffraction (XRD) was measured under Bruker D8 diffractometer using Cu Kα radiation. Raman spectrum was recorded at ambient temperature on a Renishaw Raman spectrometer with an argon-ion laser at an excitation wavelength of 532 nm. X-ray photoelectron spectroscopy (XPS) was conducted on an ESCALAB 250 instrument, using monochrome Al Kα (300.0 eV) as the excitation source.

Electrochemical Measurements. Cyclic voltammetry (CV) and electrochemical impedance spectroscopy (EIS) were performed with a CHI 760B electrochemical workstation (Chenhua, Shanghai, China). Galvanostatic (GV) charge−discharge tests were performed on potentiostat/galvanostat (CT2001A, Land, Wuhan, China). The electrodes of the supercapacitors were prepared by pressing mixtures of porous carbon sample, acetylene black, and PTFE binder (75:20:5 w/w/w) onto a stainless steel grid with an area of about 1 cm^2. Thereafter, the electrode was dried under 105 °C for 24 h. For single electrode test, a three-electrode setup in 1 mol L^{-1} H_2SO_4 was used under ambient conditions with a stainless steel grid and a Hg/Hg_2SO_4 as a counter and reference electrode, respectively. CV experiments were performed at scan rates of 2, 5, 10, 20, 50, 100, 150, and 200 mV s^{-1} at the potential range of 0 to −1 V. GV charge/discharge curves were obtained at current densities of 1, 2, 5, and 10 A g^{-1} to evaluate the specific capacitance. Particularly, when the current densities rise to 20 A g^{-1} and 30 A g^{-1}, the tests were conducted under CHI 760B electrochemical workstation. A two-electrode cell configuration was used to measure the performance of supercapacitors under the same conditions.

RESULTS AND DISCUSSION

CTAB, a cationic surfactant, plays a key role in the morphology of PNPEA. PEA molecules will settle down inside the micelles in aqueous solutions in the presence of CTAB,[24,25] and the lamellar mesostructural $(CTA)_2S_2O_8$ is formed when a certain concentration of APS solution added to the mixture. The $S_2O_8^{2-}$anions permeate into the interior of the micelles to oxidize PEA to PNPEA. The morphology of the micelles depends upon the ratio of CTAB and PEA, so CTAB is regarded as a soft template, which controls the structure and morphology of the resulting PNPEA.[26] The morphology of PNPEA is changed along with the molar ratio of CTAB and PEA. When the ratio is 1:5 (CTAB/PEA), the material surface has a rough surface and presents a cluster state (Figure S1A), and relative uniform microspheres are obtained when the ratio is decreased to 1:25 (Figure 1A); however, when the ratio changes to 1:50, microspheres disappear and blocky structure appears (Figure S1B). Thus, it is believed that the optimum ratio of CTAB to PEA is 1:25 in this case. Scheme 1 shows the probable mechanism of the peanut-shell-like porous carbon formation, which experiences three processes. First, PEA molecules and CTAB could form dumbbell shaped micelles, where PEA molecules are surrounded by CTAB ones. The hydrophilic group (quaternary amine cation) of CTAB keeps toward the water phase, and its hydrophobic group is directional to the PEA one. Second, when ammonium peroxydisulfate (APS) is added to the aqueous solution, $S_2O_8^{2-}$ anions would rapidly close to the micelles by electrostatic forces, and then the anions permeate into the interior of the micelles to oxidize PEA to PNPEA, and the peanut-like structure is produced. The peanut-like-shell could prevent further reaction between the $S_2O_8^{2-}$ anions and the interior PEA molecules. Therefore, it is reasonable to speculate that PEA in the shell would maintain the original molecule state or being oxidized to PNPEA oligomer. Third, when PNPEA sample and potassium hydroxide were pyrolysised in a tube, PEA or PNPEA oligomer inside the shell and CTAB outward the shell were decomposed into gas, and the peanut-shell-like polyporous carbon was therefore prepared.

It has been popularly accepted that the composition and morphology of the precursors play a very important role in the morphology and structure of the resulting carbon.[27−29] For example, if a precursor morphology is fibroid shape, carbon fibers could be obtained, and if a precursor morphology is nanotubular, carbon nanotube could be therefore produced. In other words, precursor morphology sometimes determines the morphology of the resulting carbon. PNPEA shows peanut morphology (Figure 1A), so it is not surprising that the carbon (PNPEA-KOH-800) presents peanut-shell-like configuration (Figure 1B).

At high magnification (Figure 1C), it has an interplanar spacing of 0.27 nm, indicating well graphitization of PNPEA-KOH-800. As illustrated in Figure 1D, the adsorption isotherm increases significantly at a low pressure area, and a clear hysteresis phenomenon happens when relative pressure exceeds 0.3, indicating PNPEA-KOH-800 is composed of both micropores and mesopores. The pore size calculated by the nonlocal density functional theory (NLDFT) method suggesting the sample has a hierarchically porous framework, where the abundant micropores are of great importance in charge

DOI: 10.1021/acsami.5b05022
ACS Appl. Mater. Interfaces 2015, 7, 22238−22245

storage capacity (the inset of Figure 1D). The mechanism of KOH activation is generally considered as a reaction between KOH and carbon.[30]

$$6KOH + 2C \rightarrow 2K + 3H_2 + 2K_2CO_3 \quad (1)$$

The reaction mechanism can be visualized as follows: (1) the dehydrating action of KOH at 500 °C, producing K_2O which is reduced to free K under a high temperature, meanwhile, the K inserts into carbon net plane layer of the microcrystalline graphite and then the adjacent carbon net plane is open and many voids form;[21] (2) K_2CO_3 begins to break drown to CO_2 and K_2O at temperature higher than 700 °C, and K_2O is also reduced to K. When K squeezes into the carbon structure, the distance of the carbon atom layer is enlarged, thus increasing the pore volume.[31]

Figure 1E shows the XRD patterns of the materials under different conditions. Before KOH activation, the strong diffraction peaks at 2θ of 24 and 43.8° correspond to the (002) and (101) planes of hexagonal carbon materials and are related to an amorphous carbon structure.[32] After activation, the two peaks almost vanished, which may be attributed to that activation process caused plentiful cavity construction, destroyed the graphite crystallite, therefore reducing the peak intensity. The electric arc caused by K^+ intercalation might also affect the graphite crystallites.[33] Raman spectrum was used to further characterize PNPEA-KOH-800. As illustrated in Figure 1F, two distinct peaks at 1355 and 1595 cm^{-1} were in coincidence with the well-documented D (defects and disorder) and G (graphitic) bands.[34]

The XPS survey spectrum shown in Figure 2A gives the information on elemental compositions and surface functionalities. It consists of three peaks located at 284.4, 399.8, and 532.8 eV, corresponding to C 1s, N 1s, and O 1s, respectively. The fitting of N 1s spectrum of PNPEA-KOH-800 (Figure 2B) shows three broad peaks at 399.8 (pyrrolic N), 400.9 (quaternary N), and 405.4 eV (pyridine N oxides), respectively.[35] In the O 1s spectrum of PNPEA-KOH-800 (Figure 2C), there are four peaks: peak 1 centered at 532.3 eV associated with C−OH groups, peak 2 at 533.3 eV ascribed to the C−O−C groups, another two relative weak peaks at 531.2 eV (C = O groups), and 534.5 eV (COOH carboxyl groups).[36] The XPS results indicate that the carbon samples have been successfully doped with heteroatom N.

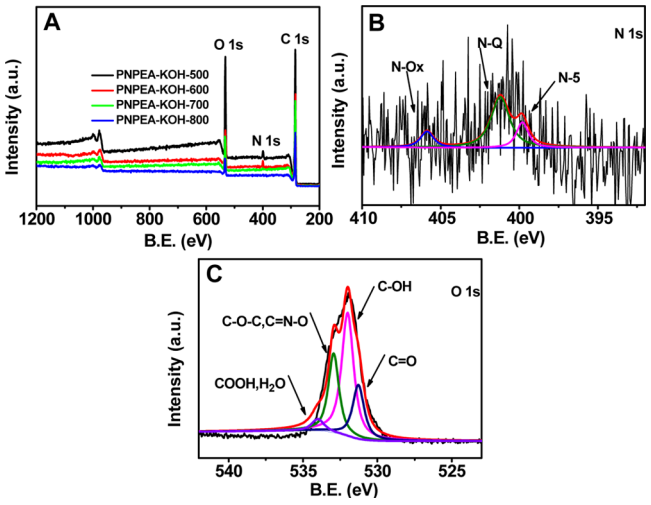

Figure 2. (A) Extensive XPS spectra of carbons derived of PNPEA; (B) high-resolution N 1s XPS spectra and fitting curve of PNPEA-KOH-800; (C) high-resolution O 1s XPS spectra of PNPEA-KOH-800.

Electrochemical performances of the obtained materials were evaluated by CV tests. Figure 3A shows that PNPEA-KOH-800 exhibits typical capacitive behavior with rectangular shaped voltammetry characteristics even at a high potential scan rate of 200 mV s^{-1}. The capacitance calculated by CV integral area indicates that PNPEA-KOH-800 has the highest capacitance, as shown in Figure 3B. The constant current GV charge/discharge curves of PNPEA-KOH-800 at different current densities were displayed in Figure 3C. During the charging and discharging steps, the charge curves exhibit a linear profile, which is almost symmetric to its corresponding discharge counterpart and can be maintained even at a low density of 0.5 A g^{-1}. It should be noted that a small IR drop is observed, which suggests that the usable voltage is often less than 1 V. Figure 3D summarizes the voltage drop under different currents. It is evident that the voltage drop increases linearly with current increase, and the slope of this linear relationship corresponds to the overall internal resistance value.[37,38]

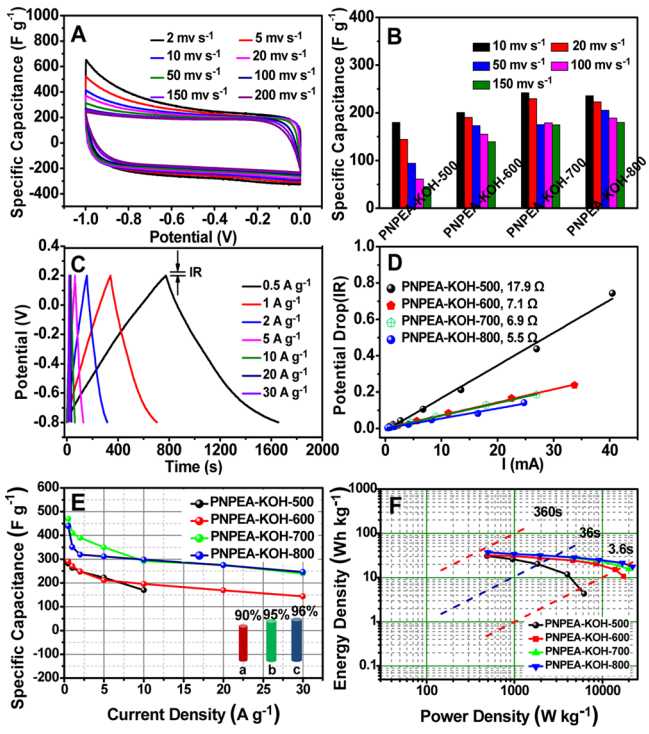

Figure 3. (A) CV curves of PNPEA-KOH-800 under different sweep rates. (B) The capacitances of PNPEA-KOH-Ts under different sweep rates. (C) Charge−discharge curves of PNPEA-KOH-800 at different current densities by three-electrode configuration. (D) The relationship between IR and *I*. (E) The specific capacitances of PNPEA-KOH-T electrodes under different current densities; capacitance retention at 30 A g^{-1} of (a) PNPAE-KOH-600, (b) PNPA-KOH-700, and (c) PNPEA-KOH-800. (F) Ragone plots about specific power against specific energy of the samples based on a two-electrode cell.

The specific capacitance (C_{sp}) was calculated using the GV charge/discharge curves of supercapacitors provided in Figure 3C and the following equation:[39]

DOI: 10.1021/acsami.5b05022
ACS Appl. Mater. Interfaces 2015, 7, 22238−22245

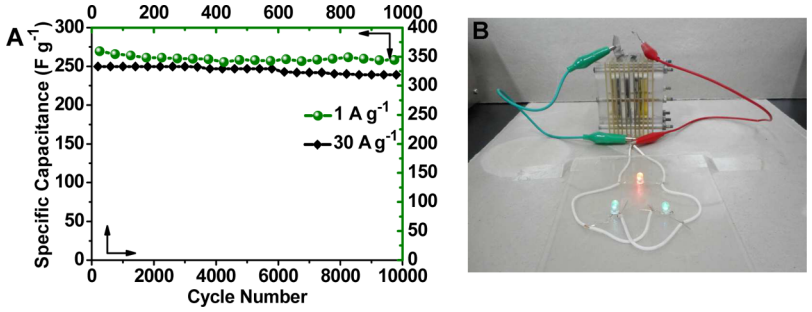

Figure 4. (A) The specific capacitance of PNPEA-KOH-800 at 1 A g^{-1} and 30 A g^{-1} in a three-electrode system; (B) the photo of three colored LEDs which were lit by three series symmetric two-electrode (PNPEA-KOH-800) capacitors.

Table 1. Summary of Structure and Capacitance of Different Samples

				atomic ratio (%)[d]				
samples	S_{BET} (m^2 g^{-1})[a]	S_{micro} (m^2 g^{-1})[b]	V_T (cm^3 g^{-1})[c]	C	O	N	I_D/I_G[e]	C (F g^{-1})[f]
PNPEA-KOH-500	956	772	1.04	77.20	19.91	2.89	0.955	173
PNPEA-KOH-600	2676	2465	1.42	82.40	14.96	2.64	1.023	196
PNPEA-KOH-700	3616	3303	1.72	85.72	13.76	0.52	1.047	292
PNPEA-KOH-800	3103	2770	1.37	88.62	10.98	0.40	1.070	298

[a]BET surface area. [b]*t*-Plot micropore area. [c]Single point adsorption total pore volume of pores at p/p_o= 0.995. [d]XPS analysis results of atomic ratio of C, O, and N. [e]Area proportion of D and G bands by Raman spectrum method. [f]Specific capacitance at 10 A g^{-1} in 1 mol L^{-1} H_2SO_4.

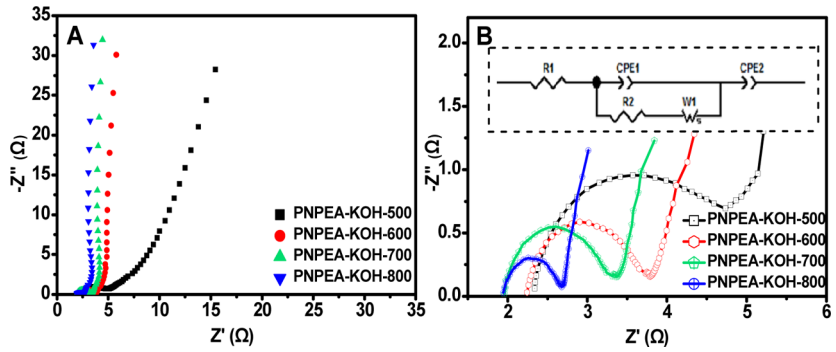

Figure 5. (A) EIS curves of PNPEA-KOH-T electrodes by two-electrode cell; (B) partial enlargement of Nyquist plots and (inset) diagram of equivalent circuit.

$$C_{sp} = \frac{I\Delta T}{m\Delta V} \quad (2)$$

where I is the constant current (A), ΔT is the discharge time (s), ΔV (V) refers to the potential change, and m is the total mass (g) of active materials in both electrodes. Figure 3E shows the variation in specific capacitance with the current density. It is obvious that as current density increases, the specific capacitance decreases. This results from the difficulties in penetration and diffusion of electrolyte ions into a poorly conductive layer and/or thick electrode films.[40] The capacitive performances of all the samples are summarized in Table S1. The specific capacitance of PNPEA-KOH-800 is 356, 320, and 312 F g^{-1} at a current density of 1, 2, and 5 A g^{-1}, respectively. Although it is slightly inferior to that of PNPEA-KOH-700, it becomes superior to that of PNPEA-KOH-700 when the current density rises up to 10 A g^{-1} (Figure S2).

Energy density (Wh kg^{-1}) and power density (kW kg^{-1}) of the fabricated supercapacitors were calculated using the following equations: [41]

$$E = \frac{1}{2}C\Delta V^2 \quad (3)$$

$$P = \frac{E}{\Delta T} \quad (4)$$

where C is the capacitance of the two-electrode capacitor (F g^{-1}), ΔV is the operation voltage ($V_{max} - IR_{drop}$), and ΔT is the discharge time (s). As shown in Figure 3F, at a time of 3.6 s, the energy and power densities of PNPEA-KOH-800 based capacitors are 20.84 Wh kg^{-1} and 19.27 KW kg^{-1}. Evidently, our sample is more advanced than many than carbon materials[42] (Table S2) and even commercial devices (3 Wh kg^{-1}).[20,43] Figure 4A shows the cycle life of PNPEA-KOH-800 at 1 and 30 A g^{-1}, and the retention rate of capacitance reaches 95% (1000 cycles). High capacitance, fast charge−discharge performance, and high retention rate of capacitance lays the groundwork for fabricating practical energy conversion devices. Figure 4B shows a digital photo of LEDs powered by cell assembled with three series symmetric two-electrode (PNPEA-KOH-800) capacitors in 1 mol L^{-1} H_2SO_4 solution, and relevant video (Supporting Information) is given to demonstrate the potential applications of our electrode materials in energy storage. The LED used here is color lamp bulb, and its working voltage and operating current are 1.8−3.4 V and 20 mA, respectively. The power for driving LED here is a galvanic

DOI: 10.1021/acsami.5b05022
ACS Appl. Mater. Interfaces 2015, 7, 22238−22245

pile consisting of three capacitor units. It is observed that after being fully charged, the three-unit capacitors can easily power three color LEDs which can be successfully illuminated for more than 11 min. In addition, we also tried four-unit capacitor device in series to drive three color LEDs, and most interestingly, the LEDs can keep light for 70 min when the device is only charged for 10 s, which far exceeds previous reports.[44−46] The capacitance performance of a supercapacitor depends on the specific surface and the (electronic and ionic) conductivity of its electrode material. Usually, high surface area and high conductivity make great contributions to excellent capacitive property. Under similar conditions such as PNPEA-KOH-700 and PNPEA-KOH-800, the surface area determines the performance of the capacitor at low discharging current density, and at high scanning rate and current density, the conductivity is the main factor for the capacitance performance. PNPEA-KOH-700 possesses the highest surface area among PNPEA-KOH-T (T stands for 500, 600, 700, and 800) samples (Table 1), so it shows the most excellent capacitive property at low discharging current density. PNPEA-KOH-800 possesses the highest conductivity among PNPEA-KOH-T samples (Figure 5B), and therefore it shows the most excellent capacitive property at high scanning rate and current density. The inferior CV character (Figure S3) and specific capacitance (Table S1) of PNPEA-KOH-500 and PNPEA-KOH-600 might be due to lower effective SSA and pore volume,[19] and the microstructure parameters were listed in Table 1. The surface area and pore volume increase with the rise in the activation temperature from 500 to 700 °C. When the activation temperature reaches 800 °C, both the surface area and pore volume decrease slightly, which may be attributed to the collapse of pores and enhanced orientation during the graphitizing process.[47−49] The higher effective SSA and pore volume of PNPEA-KOH-700 and PNPEA-KOH-800 undoubtedly result in a superior electrochemical performance. Generally speaking, when the I_D/I_G is approximately 1.0, the carbon materials become amorphous.[50,51] The increase of the activation temperature results in the growth of I_D/I_G ratio (Figure S4), indicating a slight increase of disordering, which is consistent with XRD results. The pyrrolic and pyridinic nitrogen species from doping heteroatoms can make partial contribution to the capacity (Figure S5).[30] And activation temperature has a great influence on chemistry composition and content, especially the mass ratio of nitrogen decreases gradually with the temperature rising.[52] Thus, pyrolysis and activation temperature can tune the capacity.

EIS is an effective method to evaluate the transport properties of the supercapacitors. When the electrode process was controlled by both charge−transfer process and ion diffusion process, the Nyquist plot was constructed by a semicircle in the high-frequency region[53,54] and a sloped line in the low-frequency region,[55] as shown in Figure 5, which was measured in 1 mol L^{-1} H_2SO_4 solution in the range of 10 mHz to 100 kHz at an applied potential of 0 V with sinusoidal signal of 5 mV. Among all the samples, at high frequencies, PNPEA-KOH-800 owns the smallest loop, indicating the lowest ion adsorption efficiency and fastest ion diffusion/transport.[51] The straight line along the imaginary axis at low frequency reveals fast ion diffusion/transport in the electrolyte to the electrode surface.[56] The impedance plot of PNPEA-KOH-800 was more vertical than the other samples, and its semicircle is smaller, indicating a smaller interfacial charge transfer resistance (~0.756 Ω), as summarized in Table 2. It is reasonable that

Table 2. Parameters of Equivalent Circuit of Different Samples for the Two-electrode System

samples	R_t (Ω)[a]	R_s (Ω)[b]	R_{ct} (Ω)[c]	R_p (Ω)[d]
PNPEA-KOH-500	4.931	2.341	2.392	0.198
PNPEA-KOH-600	3.962	2.244	1.567	0.151
PNPEA-KOH-700	3.415	1.958	1.408	0.049
PNPEA-KOH-800	2.723	1.946	0.756	0.021

[a]Total resistance. [b]Solution resistance. [c]Charge transfer resistance. [d]Equivalent distributed pore resistance.

PNPEA-KOH-800 possesses the remarkable capacitor performance. The results are consistent with previous analysis. Also, according to eq 3, the smaller the internal resistance, the better the performance, especially at a fast discharge rate. PEA-KOH-800 possesses lower internal resistance and bigger size pores, promoting ion diffusion,[19,57] thus having superior energy density and power density.

All the factors posing effect on the electrochemical properties discussed above were compiled in Figure 6. PNPEA-KOH-700

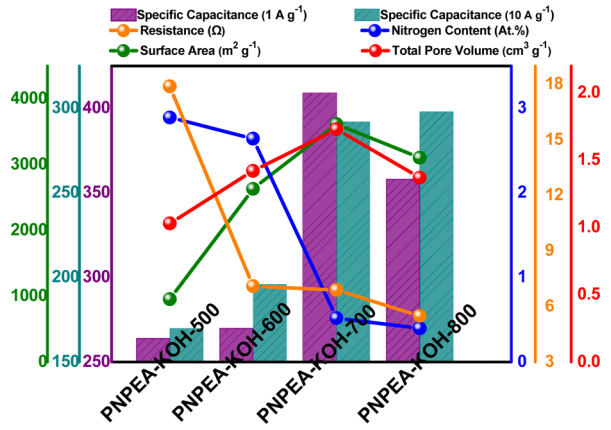

Figure 6. Effects of surface area, specific capacitance, nitrogen content, resistance, total pore volume on electrochemical properties of PNPEA-KOH-Ts.

shows an excellent capacitive property at 1 A g^{-1} owing to higher surface area and a certain amount of nitrogen concentration, nevertheless, seems to be a more promising electrode material at high scanning rate and current density. No one factor can dominate the material, but there's a balance among SSA, total pore volume, nitrogen content, and resistance to achieve an excellent electrochemical performance.

CONCLUSIONS

In summary, we have demonstrated a series of N-doped porous carbon materials via carbonization and activation of PNPEA. These products especially synthesized under higher temperature have a good performance in terms of specific capacitance, capacitance retention, and internal resistance. PNPEA-KOH-700 exhibits the highest capacity of 409 and 264 F g^{-1} at a current density of 1 A g^{-1} in three-electrode system and two-electrode cell configuration, respectively. The material carbonized at 800 °C displays a high rate performance with a specific capacitance of 249 F g^{-1} at 30 A g^{-1}, which exceeds 240 F g^{-1} of PNPEA-KOH-700, and have a good stability after 10 000 cycles. It is not difficult to explain that PNPEA-KOH-800 owns lower internal resistance, high effective surface area, heteroatom doping effects and lower resistance. A combination of these

DOI: 10.1021/acsami.5b05022
ACS Appl. Mater. Interfaces 2015, 7, 22238−22245

advantages will take our samples to find extensive utilizations in supercapacitors.

■ ASSOCIATED CONTENT

Supporting Information

The Supporting Information is available free of charge on the ACS Publications website at DOI: 10.1021/acsami.5b05022.

SEM images of PNPEA under different molar ratio of CTAB and PEA, Ar or N_2 adsorption−desorption isotherms, Raman spectra, XPS spectra, CV curves under different sweep rates and cycle life of PNPEA-KOH-Ts under different current densities, and the supercapacitor performance of different activated carbons reported in the literatures. (PDF)

Video of application of electrode materials in energy storage. (AVI)

■ AUTHOR INFORMATION

Corresponding Authors

*E-mail: xj_wei@163.com.

*E-mail: shuyangao@htu.cn.

Author Contributions

The manuscript was written through contributions of all authors. All authors have given approval to the final version of the manuscript.

Notes

The authors declare no competing financial interest.

■ ACKNOWLEDGMENTS

This work is supported by NSFCs (21471048), the Research Project of Chinese Ministry of Education (No. 213023A), NCET-11-0944, the Excellent Youth Foundation of Henan Scientific Committee (124100510004), the Program for Innovative Research Team in University of Henan Province (No. 14IRTSTHN005), and the Program for Science& Technology Innovation Talents in Universities of Henan Province (2011HASTIT010), which are gratefully acknowledged. Dr. Hua Zhong from Micromeritics Instrument (Shanghai) Ltd. is greatly appreciated for her help with BET analysis using *t*-plot method.

■ REFERENCES

(1) Yang, H.; Shi, Q.; Liu, X.; Xie, S.; Jiang, D.; Zhang, F.; Yu, C.; Tu, B.; Zhao, D. Synthesis of Ordered Mesoporous Carbon Monoliths with Bicontinuous Cubic Pore Structure of Ia3dSymmetry. *Chem. Commun.* **2002**, *23*, 2842−2843.

(2) Kong, L.; Wei, W.; Zhao, Q.; Wang, J.-Q.; Wan, Y. Active Coordinatively Unsaturated Manganese Monoxide-containing Mesoporous Carbon Catalyst in Wet Peroxide Oxidation. *ACS Catal.* **2012**, *2*, 2577−2586.

(3) Dai, L.; Chang, D. W.; Baek, J.-B.; Lu, W. Carbon Nanomaterials for Advanced Energy Conversion and Storage. *Small* **2012**, *8*, 1130−1166.

(4) Gauthier, E.; Hellstern, T.; Kevrekidis, I. G.; Benziger, J. Drop Detachment and Motion on Fuel Cell Electrode Materials. *ACS Appl. Mater. Interfaces* **2012**, *4*, 761−771.

(5) Dutta, S.; Bhaumik, A.; Wu, K. C.-W. Hierarchically Porous Carbon Derived from Polymers and Biomass: Effect of Interconnected Pores on Energy Applications. *Energy Environ. Sci.* **2014**, *7*, 3574−3592.

(6) Zheng, X.; Lv, W.; Tao, Y.; Shao, J.; Zhang, C.; Liu, D.; Luo, J.; Wang, D.-W.; Yang, Q.-H. Oriented and Interlinked Porous Carbon Nanosheets with an Extraordinary Capacitive Performance. *Chem. Mater.* **2014**, *26*, 6896−6903.

(7) Chen, T.; Dai, L. Carbon Nanomaterials for High-performance Supercapacitors. *Mater. Today* **2013**, *16*, 272−280.

(8) Kierzek, K.; Frackowiak, E.; Lota, G.; Gryglewicz, G.; Machnikowski, J. Electrochemical Capacitors Based on Highly Porous Carbons Prepared by KOH Activation. *Electrochim. Acta* **2004**, *49*, 515−523.

(9) Rufford, T. E.; Hulicova-Jurcakova, D.; Khosla, K.; Zhu, Z.; Lu, G. Q. Microstructure and Electrochemical Double-layer Capacitance of Carbon Electrodes Prepared by Zinc Chloride Activation of Sugar Cane Bagasse. *J. Power Sources* **2010**, *195*, 912−918.

(10) Sevilla, M.; Valle-Vigón, P.; Fuertes, A. B. N-doped Polypyrrole-based Porous Carbons for CO_2 Capture. *Adv. Funct. Mater.* **2011**, *21*, 2781−2787.

(11) Lozano-Castelló, D.; Cazorla-Amorós, D.; Linares-Solano, A.; Quinn, D. F. Influence of Pore Size Distribution on Methane Storage at Relatively Low Pressure: Preparation of Activated Carbon with Optimum Pore Size. *Carbon* **2002**, *40*, 989−1002.

(12) Sevilla, M.; Parra, J. B.; Fuertes, A. B. Assessment of the Role of Micropore Size and N-doping in CO_2 Capture by Porous Carbons. *ACS Appl. Mater. Interfaces* **2013**, *5*, 6360−6368.

(13) Lv, Y.; Zhang, F.; Dou, Y.; Zhai, Y.; Wang, J.; Liu, H.; Xia, Y.; Tu, B.; Zhao, D. A Comprehensive Study on KOH Activation of Ordered Mesoporous Carbons and Their Supercapacitor Application. *J. Mater. Chem.* **2012**, *22*, 93−99.

(14) Wang, Z. L.; Kang, Z. C. Graphitic Structure and Surface Chemical Activity of Nanosize Carbon Spheres. *Carbon* **1997**, *35*, 419−426.

(15) Zhao, L.; Fan, L.-Z.; Zhou, M.-Q.; Guan, H.; Qiao, S.; Antonietti, M.; Titirici, M.-M. Nitrogen-containing Hydrothermal Carbons with Superior Performance in Supercapacitors. *Adv. Mater.* **2010**, *22*, 5202−5206.

(16) Ferrero, G. A.; Fuertes, A. B.; Sevilla, M. N-doped Porous Carbon Capsules with Tunable Porosity for High-performance Supercapacitors. *J. Mater. Chem. A* **2015**, *3*, 2914−2923.

(17) Seredych, M.; Hulicova-Jurcakova, D.; Lu, G. Q.; Bandosz, T. J. Surface Functional Groups of Carbons and the Effects of Their Chemical Character, Density and Accessibility to Ions on Electrochemical Performance. *Carbon* **2008**, *46*, 1475−1488.

(18) Kim, Y. J.; Abe, Y.; Yanagiura, T.; Park, K. C.; Shimizu, M.; Iwazaki, T.; Nakagawa, S.; Endo, M.; Dresselhaus, M. S. Easy Preparation of Nitrogen-enriched Carbon Materials from Peptides of Silk Fibroins and Their Use to Produce a High Volumetric Energy Density in Supercapacitors. *Carbon* **2007**, *45*, 2116−2125.

(19) Qian, W.; Sun, F.; Xu, Y.; Qiu, L.; Liu, C.; Wang, S.; Yan, F. Human Hair-derived Carbon Flakes for Electrochemical Supercapacitors. *Energy Environ. Sci.* **2014**, *7*, 379−386.

(20) Gogotsi, Y.; Simon, P. True Performance Metrics in Electrochemical Energy Storage. *Science* **2011**, *334*, 917−918.

(21) Zhu, Y.; Murali, S.; Stoller, M. D.; Ganesh, K. J.; Cai, W.; Ferreira, P. J.; Pirkle, A.; Wallace, R. M.; Cychosz, K. A.; Thommes, M.; Su, D.; Stach, E. A.; Ruoff, R. S. Carbon-based Supercapacitors Produced by Activation of Graphene. *Science* **2011**, *332*, 1537−1541.

(22) Gao, Y.; Zhang, W.; Yue, Q.; Gao, B.; Sun, Y.; Kong, J.; Zhao, P. Simple Synthesis of Hierarchical Porous Carbon from Enteromorpha Prolifera by a Self-template Method for Supercapacitor Electrodes. *J. Power Sources* **2014**, *270*, 403−410.

(23) Wang, Y.; Yang, R.; Li, M.; Zhao, Z. Hydrothermal Preparation of Highly Porous Carbon Spheres from Hemp (Cannabis sativa L.) Stem Hemicellulose for Use in Energy-related Applications. *Ind. Crops Prod.* **2015**, *65*, 216−226.

(24) Mao, H.; Lu, X. F.; Chao, D. M.; Cui, L. L.; Zhang, W. J. Controlled Growth of Poly (N-methylaniline): From Nanowires to Microspheres. *Mater. Lett.* **2008**, *62*, 998−1001.

(25) Zhang, X. T.; Zhang, J.; Liu, Z. F.; Robinson, C. Inorganic/Organic Mesostructure Directed Synthesis of Wire/Ribbon-like Polypyrrole Nanostructures. *Chem. Commun.* **2004**, *16*, 1852−1853.

DOI: 10.1021/acsami.5b05022
ACS Appl. Mater. Interfaces 2015, 7, 22238−22245

(26) Hu, X. X.; Bao, H.; Wang, P.; Jin, S. L.; Gu, Z. M. Mechanism of Formation of Polyaniline Flakes with High Degree of Crystallization Using a Soft Template in the Presence of Cetyltrimethy-lammonium Bromide. *Polym. Int.* **2012**, *61*, 768−773.
(27) Zhang, W. X.; Liu, J.; Wu, G. Evolution of Structure and Properties of PAN Precursors During Their Conversion to Carbon Fibers. *Carbon* **2003**, *41*, 2805−2812.
(28) Tin, P. S.; Xiao, Y. C.; Chung, T.-S. Polyimide-carbonized Membranes for Gas Separation: Structural, Composition, and Morphological Control of Precursors. *Sep. Purif. Rev.* **2006**, *35*, 285−318.
(29) Langer, J. J.; Golczak, S. Highly Carbonized Polyaniline Micro- and Nanotubes. *Polym. Degrad. Stab.* **2007**, *92*, 330−334.
(30) Yun, Y. S.; Cho, S. Y.; Shim, J.; Kim, B. H.; Chang, S.-J.; Baek, S. J.; Huh, Y. S.; Tak, Y.; Park, Y. W.; Park, S.; Jin, H.-J. Microporous Carbon Nanoplates from Regenerated Silk Proteins for Supercapacitors. *Adv. Mater.* **2013**, *25*, 1993−1998.
(31) Wang, H.; Gao, Q.; Hu, J. High Hydrogen Storage Capacity of Porous Carbons Prepared by Using Activated Carbon. *J. Am. Chem. Soc.* **2009**, *131*, 7016−7022.
(32) Zhai, Y.; Dou, Y.; Zhao, D.; Fulvio, P. F.; Mayes, R. T.; Dai, S. Carbon Materials for Chemical Capacitive Energy Storage. *Adv. Mater.* **2011**, *23*, 4828−4850.
(33) Mora, E.; Blanco, C.; Pajares, J. A.; Santamaria, R.; Menéndez, R. Chemical Activation of Carbon Mesophase Pitches. *J. Colloid Interface Sci.* **2006**, *298*, 341−347.
(34) Ji, L.; Zhang, X. Electrospun Carbon Nanofibers Containing Silicon Particles as an Energy-storage Medium. *Carbon* **2009**, *47*, 3219−3226.
(35) Zhang, C.; Fu, L.; Liu, N.; Liu, M.; Wang, Y.; Liu, Z. Synthesis of Nitrogen-doped Graphene Using Embedded Carbon and Nitrogen Sources. *Adv. Mater.* **2011**, *23*, 1020−1024.
(36) Hulicova-Jurcakova, D.; Seredych, M.; Lu, G. Q.; Bandosz, T. J. Combined Effect of Nitrogen- and Oxygen-containing Functional Groups of Microporous Activated Carbon on its Electrochemical Performance in Supercapacitors. *Adv. Funct. Mater.* **2009**, *19*, 438−447.
(37) Izadi-Najafabadi, A.; Yasuda, S.; Kobashi, K.; Yamada, T.; Futaba, D. N.; Hatori, H. Extracting the Full Potential of Single-walled Carbon Nanotubes as Durable Supercapacitor Electrodes Operable at 4 V with High Power and Energy Density. *Adv. Mater.* **2010**, *22*, E235−E241.
(38) Yang, X.; Zhang, L.; Zhang, F.; Zhang, T.; Huang, Y.; Chen, Y. A High-performance All-solid-state Supercapacitor with Graphene-doped Carbon Material Electrodes and a Graphene Oxide-doped Ion Gel Electrolyte. *Carbon* **2014**, *72*, 381−386.
(39) Wang, R.; Wang, P.; Yan, X.; Lang, J.; Peng, C.; Xue, Q. Promising Porous Carbon Derived from Celtuce Leaves with Outstanding Supercapacitance and CO_2 Capture Performance. *ACS Appl. Mater. Interfaces* **2012**, *4*, 5800−5806.
(40) Yuksel, R.; Sarioba, Z.; Cirpan, A.; Hiralal, P.; Unalan, H. E. Transparent and Flexible Supercapacitors with Single Walled Carbon Nanotube Thin Film Electrodes. *ACS Appl. Mater. Interfaces* **2014**, *6*, 15434−15439.
(41) Hao, Q.; Xia, X.; Lei, W.; Wang, W.; Qiu, J. Facile Synthesis of Sandwich-like Polyaniline/boron-doped Graphene Nano Hybrid for Supercapacitors. *Carbon* **2015**, *81*, 552−563.
(42) Zheng, C.; Qi, L.; Yoshio, M.; Wang, H. Cooperation of Micro- and Meso-porous Carbon Electrode Materials in Electric Double-layer Capacitors. *J. Power Sources* **2010**, *195*, 4406−4409.
(43) Qu, Q.; Li, L.; Tian, S.; Guo, W.; Wu, Y.; Holze, R. A Cheap Asymmetric Supercapacitor with High Energy at High Power: Activated Carbon/$K_{0.27}MnO_2{\cdot}0.6H_2O$. *J. Power Sources* **2010**, *195*, 2789−2794.
(44) Song, Y.; Cai, X.; Xu, X. X.; Liu, X. X. Integration of Nickel−cobalt Double Hydroxide Nanosheets and Polypyrrole Films with Functionalized Partially Exfoliated Graphite for Asymmetric Supercapacitors with Improved Rate Capability. *J. Mater. Chem. A* **2015**, *3*, 14712−14720.
(45) Wang, D. W.; Min, Y. G.; Yu, Y. H. Facile Synthesis of Wheat Bran-derived Honeycomb-like Hierarchical Carbon for Advanced Symmetric Supercapacitor Applications. *J. Solid State Electrochem.* **2015**, *19*, 577−584.
(46) Cao, J. Y.; Wang, Y. M.; Chen, J. C.; Li, X. H.; Walsh, F. C.; Ouyang, J. H.; Jia, D. C.; Zhou, Y. Three-dimensional Graphene Oxide/polypyrrole Composite Electrodes Fabricated by One-step Electrodeposition for High Performance Supercapacitors. *J. Mater. Chem. A* **2015**, *3*, 14445−14457.
(47) Zhu, H.; Wang, X.; Liu, X.; Yang, X. Integrated Synthesis of Poly (o-phenylenediamine)-derived Carbon Materials for High Performance Supercapacitors. *Adv. Mater.* **2012**, *24*, 6524−6529.
(48) Lee, J. S.; Wang, X.; Luo, H.; Baker, G. A.; Dai, S. Facile Ionothermal Synthesis of Microporous and Mesoporous Carbons from Task Specific Ionic liquids. *J. Am. Chem. Soc.* **2009**, *131*, 4596−4597.
(49) Lee, J. S.; Wang, X.; Luo, H.; Dai, S. Fluidic Carbon Precursors for Formation of Functional Carbon under Ambient Pressure Based on Ionic Liquids. *Adv. Mater.* **2010**, *22*, 1004−1007.
(50) Liu, M.; Gan, L.; Xiong, W.; Zhao, F.; Fan, X.; Zhu, D.; Xu, Z.; Hao, Z.; Chen, L. Nickel-doped Activated Mesoporous Carbon Microspheres with Partially Graphitic Structure for Supercapacitors. *Energy Fuels* **2013**, *27*, 1168−1173.
(51) Ma, X.; Gan, L.; Liu, M.; Tripathi, P. K.; Zhao, Y.; Xu, Z.; Zhu, D.; Chen, L. Mesoporous Size Controllable Carbon Microspheres and Their Electrochemical Performances for Supercapacitor Electrodes. *J. Mater. Chem. A* **2014**, *2*, 8407−8415.
(52) Stanczyk, K.; Dziembaj, R.; Piwowarska, Z.; Witkowski, S. Transformation of Nitrogen Structures in Carbonization of Model Compounds Determined by XPS. *Carbon* **1995**, *33*, 1383−1392.
(53) Liang, J.; Chen, S.; Xie, M.; Wang, Y.; Guo, X.; Guo, X.; Ding, W. Expeditious Fabrication of Flower-like Hierarchical Mesoporous Carbon Superstructures as Supercapacitor Electrode Materials. *J. Mater. Chem. A* **2014**, *2*, 16884−16891.
(54) Liang, Y.; Li, Z.; Fu, R.; Wu, D. Nanoporous Carbons with a 3D Nanonetwork-interconnected 2D Ordered Mesoporous Structure for Rapid Mass Transport. *J. Mater. Chem. A* **2013**, *1*, 3768−3773.
(55) Puthusseri, D.; Aravindan, V.; Madhavi, S.; Ogale, S. 3D Microporous Conducting Carbon Beehive by Single Step Polymer Carbonization for High Performance Supercapacitors: the Magic of in Situ Porogen Formation. *Energy Environ. Sci.* **2014**, *7*, 728−735.
(56) Wang, S.; Liu, R.; Han, C.; Wang, J.; Li, M.; Yao, J.; Li, H.; Wang, Y. A Novel Strategy to Synthesize Hierarchical Porous Carbohydrate-derived Carbon with Tunable Properties. *Nanoscale* **2014**, *6*, 13510−13517.
(57) Sevilla, M.; Fuertes, A. B. Direct Synthesis of Highly Porous Interconnected Carbon Nanosheets and Their Application as High Performance Supercapacitors. *ACS Nano* **2014**, *8*, 5069−5078.

DOI: 10.1021/acsami.5b05022
ACS Appl. Mater. Interfaces 2015, 7, 22238−22245